Research Square

Preprints are preliminary reports that have not undergone peer review.
They should not be considered conclusive, used to inform clinical practice,
or referenced by the media as validated information.

Radioactive disequilibrium chronometry of uranium and radium loss from weathering gold mine tailings in tropical Ghana

Collins Awuah

collins.awuah.stu@uenr.edu.gh

Tomsk Polytechnic University

Rhoda Ansuaa

National Research University Higher School of Economics

Valentina S. Yakovleva

Tomsk Polytechnic University

Research Article

Keywords: Radioactive disequilibrium, Ghana, Naturally occurring radioactive material, Mine tailings, Alpha recoil

Posted Date: November 16th, 2026

DOI: https://doi.org/10.21203/rs.3.rs-11614731/v1

License: This work is licensed under a Creative Commons Attribution 4.0 International License.
Read Full License

Additional Declarations: No competing interests reported.

Title Page

Collins Awuah[1,2*], Rhoda Ansuaa[3], Valentina Stanislavovna Yakovleva[1]

Radioactive disequilibrium chronometry of uranium and radium loss from weathering gold mine tailings in tropical Ghana

[1]*Tomsk Polytechnic University, School of Nuclear Science and Engineering, 634050, Tomsk – Russia*

[2]*University of Energy and Natural Resources, Department of Chemical Sciences, P.O. Box 214, Sunyani, Ghana*

[3]*National Research University Higher School of Economics, Faculty of Social Sciences, 101000, Moscow, Russia*

*** Corresponding Author Email:** collins.awuah.stu@uenr.edu.gh

Radioactive disequilibrium chronometry of uranium and radium loss from weathering gold mine tailings in tropical Ghana

Collins Awuah[1,2*], Rhoda Ansuaa[3], Valentina Stanislavovna Yakovleva[1]

[1]*Tomsk Polytechnic University, School of Nuclear Science and Engineering, 634050, Tomsk – Russia*

[2]*University of Energy and Natural Resources, Department of Chemical Sciences, P.O. Box 214, Sunyani, Ghana*

[3]*National Research University Higher School of Economics, Faculty of Social Sciences, 101000, Moscow, Russia*

Abstract

Radiological surveys of gold tailings can only provide activity concentrations, and not indicate whether uranium and radium are being lost. On a 1–49 year chronosequence of 54 Ghanaian tailings, $^{226}Ra/^{238}U$ rose from 1.02 to 1.44 and $^{228}Ra/^{232}Th$ fell from 1.02 to 0.92. Loss rate constants derived from these chronometers are 1.7–2.2 × 10−2 y^{-1} for uranium and 1.0–1.3 × 10^{-2} y^{-1} for radium, a little higher than the measured losses, though the numbers are still subject to uncertainty and are treated as upper limits. Leachate $^{234}U/^{238}U$, determined using alpha spectrometry, rose from 1.05 (acid-reactive) to 1.29 (oxide-rich) tailings, which falls within the range of 1.27–1.38 reported for local groundwater. Radionuclide mobility is determined by the weathering stage rather than the activity level.

Keywords

Radioactive disequilibrium · Ghana · Naturally occurring radioactive material · Mine tailings · Alpha recoil

Introduction

For several years Ghana has been the biggest gold producer in Africa [1]. The majority of the ore is run through a mill to produce silt, cyanide-leached in the processing plant and then discharged to tailings storage facilities (TSFs), where it remains for decades. Tailings are a potential long-term hazard because of the risk of dam failure, the generation of dust and leaching [2, 3] and in sulfide-bearing ores, the oxidation of pyrite and arsenopyrite can also cause acid generation,

dissolution of carbonates and precipitation of secondary Fe(III) phases [4–6]. The decay series of ^{238}U and ^{232}Th and ^{40}K are also present in gold ores. Milling does not concentrate these nuclides, but it does decrease the grain size and expose new surfaces and alter the chemical availability of these nuclides [7]. The mean activity concentration of ^{238}U in Witwatersrand tailings is approximately 785 Bq kg^{-1} [8, 9] and in tailings at Geita, Tanzania, it is approximately 70 Bq kg^{-1} of ^{226}Ra [10]. In Ghana, the radiochemical analysis of gold residues has involved neutron activation analysis of Au and As in tailings [11] and gamma-spectrometric surveys around Tarkwa [12] and Bogoso and the Perseus concession [13–15] which indicated activities close to the world soil averages and doses below the public limit. The body of work also identified $^{234}U/^{238}U$ activity ratios between 1.27 and 1.38 in water from domestic sources around the Obuasi mine [16], which is a clear indicator that uranium is being mobilised in this district, although the source of this mobilisation has not been identified. The dose index of total activity [17, 18] applies to external gamma exposure. They do not indicate whether uranium or radium is being removed from the tailings in water and they tacitly assume that a single sampling of a deposit is representative of the life of the deposit. The example of uranium mill tailing materials demonstrates this as uranium is largely associated with Fe oxyhydroxides and clays and Ra is associated with sulfates and barite; both are released and/or captured as these phases form and transform [19 – 24]. These losses can be recorded by the radioactive disequilibrium between parent and daughter elements, and the two isotopes of radium (half-lives 1600 years and 5.75 years) integrate them over vastly different periods. The above-mentioned chronometers have been applied to estimate the weathering rates on soils and weathering profiles of different time scales [25–27] but to our knowledge these chronometers have not been used together in mine residues where the time since deposition is known independently. The weathering of tailings should be faster under tropical conditions. The annual rainfall of 1400–2000 mm in southern Ghana [28], coupled with many wettings and dryings of the tailing surfaces, is contrasted with the majority of tailing weathering studies, which are conducted in temperate and semi-arid regions [4, 29–31]. There are no studies on radioactive disequilibrium and mobility of U- and Th-series nuclides in the tailings of Ghana; however, arsenic and metal enrichment around mines has been documented at Obuasi and Tarkwa, respectively [32-35]. Radioactive concentrations and doses in these tailings have been reported at some places in Ghana [11-15] through gamma-spectrometric survey. The main objective of this study is to convert the radioactive disequilibrium to a quantitative parameter for radionuclide loss by applying a

chronosequence of tailings with known ages. Its goals were: (i) to describe the mineralogical evolution of tropical gold tailings over 50 years; (ii) to develop first-order loss rate constants for U and Ra using the combination of a long lived chronometer, $^{226}Ra/^{238}U$ (t1/2(^{226}Ra) = 1600 years), and a short-lived chronometer, $^{228}Ra/^{232}Th$ (t1/2(^{228}Ra) = 5.75 years); (iii) to use alpha spectrometry to determine $^{234}U/^{238}U$ in solids and leachates to identify the mechanism of U release at each weathering stage; and (iv) to test whether U leachability can be predicted from routine laboratory measurements. The novelty is in the implementation of a combination of three disequilibrium systems whose ages of deposition are already known. The approach can be applied to any NORM waste with known deposition history, such as phosphogypsum stacks, bauxite residue or coal ash ponds, as the initial state (secular equilibrium) can be confirmed in fresh tailings.

Theory

The theoretical basis for this study is the use of radioactive disequilibrium as a proxy for the mobility of radionuclides in post-depositional weathering of mine tailings. If a decay series is initially in equilibrium, the activities of the daughter and the parent radionuclides will be equal, and the equilibrium will be destroyed by chemical fractionation due to a difference in geochemical behavior and mineralogical association between uranium, thorium and radium. Thus, deviations in the secular equilibrium of the $^{226}Ra/^{238}U$ and $^{228}Ra/^{232}Th$ ratios are used to identify the relative mobilisation and retention of radium to its parent nuclei and their different half-lives enable their sensitivity to processes integrated over different time-scales. The variations in these ratios can then be analysed in terms of radioactive growth and decay relationships, with the assumption that the initial activity ratio is known, that there are no significant external inputs of radionuclides and that the post-depositional transport is suitably limited. In addition, disequilibrium between the uranium isotopes ^{234}U and ^{238}U can be used to gain insight into uranium mobilisation because of preferential release of ^{234}U due to alpha recoil damage and preferential leaching of recoil-implanted ^{234}U from mineral surfaces. These complementary disequilibrium systems can be correlated with independently determined ages of tailing deposition and the mineral phase characterisation to

allow the distinction of radionuclide loss from mineral phase retention and the estimation of apparent first-order mobilisation rates.

Experimental

Study area and sampling

Samples were taken from three gold districts in the south of Ghana (Fig. 1). The Obuasi; located in the Ashanti belt, where gold is found in association with arsenopyrite, pyrite and carbonate alteration, and is a Paleoproterozoic Birimian lode system [36]. Tarkwa; located in the Tarkwa–Prestea belt, where there is Tarkwaian quartz-pebble conglomerates with detrital hematite, magnetite and heavy minerals [37] as well as Birimian lodes with sulfides along the Prestea–Bogoso structure [38]. New Abirem in the Akyem belt; hosting a Birimian shear-hosted system which has been in production since 2013. The average annual rainfall is approximately 1900 mm at Tarkwa, 1600 mm at Obuasi and 1500 mm at New Abirem [28]. All operations employed carbon-in-leach cyanidation, using lime to control pH, and sub-aerial deposition.

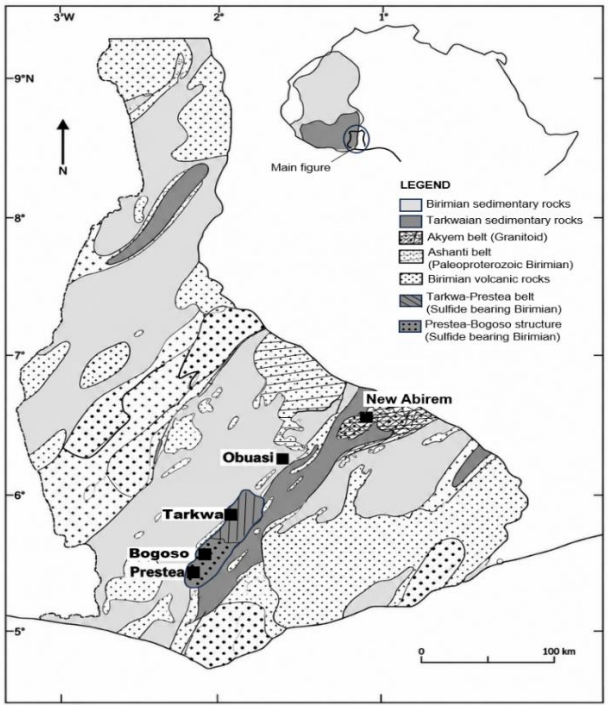


Fig. 1 Location of the sampled tailings districts in southern Ghana. (modified after Pigois et al. [37]).

A chronosequence of deposits was developed using the date of deposition information from the mines and verified from Landsat imagery 1986 to 2024. The ages of deposits are only approximate and range from about ±0.5 y based on imagery, and ±2 y based on records alone for deposits dated prior to 1986. The age classes were young (<5 y), intermediate (5-20 y) and aged (>20 y). As the Akyem TSF was commissioned in 2013, samples of aged tailings were taken in only two locations (Obuasi and Tarkwa–Prestea). The set comprised 54 samples (20 young, 20 intermediate, 14 aged), with ages of 1.1–4.5, 5.5–18.5 and 21.5–48.8 y. The dry season sampling was conducted from November 2024 to February 2025. Representative sub-samples were taken from each of the 0 to 30 cm depth layer from within a 5 m x 5 m square and bulked at each site, at least 50 m from dam walls and decant structures, to produce about 3 kg samples for each composite. Six samples (11 %) were taken as field duplicates and equipment blanks (acid washed quartz sand) were processed with each ten samples. Samples were air-dried below 40 °C, sieved to <2 mm and for chemical and mineralogical work milled to <75 μm in agate.

Physicochemical and mineralogical characterisation

The pH and electrical conductivity (EC) of the tailings–water suspensions were measured at 1:1 tailing–water ratio [39] while moisture was gravimetrically determined at 105 °C and grain size was determined by laser diffraction (Malvern Mastersizer 3000). Fused beads (Malvern Panalytical Zetium) were used for WD-XRF analysis of the major oxides. Total S was determined by combustion (LECO CS-844) and Ssulfate was determined by difference between the total S and sulfide S which was determined by chromium reduction [40]. A sulfate oxidation index was calculated as SOI = Ssulfate/Stotal. Dark extraction with acid ammonium oxalate was used to extract poorly crystalline Fe (Feo) [41]. The concentrations of As, U and Th were measured by ICP-MS (Agilent 7900) following lithium metaborate fusion. The mineral phases were semi-quantified via XRD (Bruker D8 Advance, Cu Kα, 5–70° 2θ) combined with the TOPAS 6 Rietveld program, with a 10 wt% corundum spike being used to determine the X-ray amorphous fraction. SEM-EDS (FEI Quanta 650 FEG, Bruker XFlash 6, 20 kV) was used to examine polished sections of 12 samples. Progress of weathering was summarised using a Tailing Weathering Index:

$$TWI = SOI \times (Gt + Jrs + 0.1Feo) / (Gt + Jrs + 0.1Feo + Py + Apy) \quad (1)$$

In the equation, Gt, Jrs, Py and Apy are the contents (wt%) of goethite, jarosite, pyrite and arsenopyrite, respectively, and Feo is the amount of Fe (g kg^{-1}).

Hematite was not included because it is detrital in the Tarkwa–Prestea samples. The TWI can be anywhere between 0 (fresh) and 1 (sulfide free, fully oxidised). Jarosite was below the detection limit in all samples, so its term is zero for this data set; it is retained in the index so that the TWI can be applied to more acidic tailings.

High-resolution gamma-ray spectrometry

Approximately 350 g of each of the samples with < 2 mm was packed in 300 cm3 polypropylene containers and stored for 30 days, hermetically sealed. The radon tightness was checked by recounting six containers after 45 days, and the ^{214}Pb and ^{214}Bi activities agreed with the 30-day values within 2.3 %, confirming that the containers were radon-tight. A p-type coaxial HPGe detector (40 % relative efficiency, 1.85 keV FWHM at 1332 keV) was used in a 10 cm lead shield, with Cd and Cu shielding, to obtain spectra for 86,400 s. Efficiencies were calibrated in the same geometry for the three reference materials IAEA RGU-1, RGTh-1 and RGK-1 and then transferred to all the sample densities (0.98–1.61 g cm^{-3}) and compositions with EFFTRAN [42] to obtain full-energy-peak efficiencies, with true-coincidence summing corrections applied to ^{214}Bi, ^{228}Ac and ^{208}Tl. ^{238}U was determined from 234Th (63.3 keV, with transmission-based self-absorption correction [43]) and ^{234m}Pa (1001.0 keV); ^{226}Ra from ^{214}Pb (295.2, 351.9 keV) and ^{214}Bi (609.3 keV); ^{228}Ra from ^{228}Ac (911.2, 969.0 keV); ^{228}Th from ^{212}Pb (238.6 keV) and ^{208}Tl (583.2 keV); and ^{40}K from 1460.8 keV. The ICP-MS Th concentration (1 mg kg^{-1} = 4.06 Bq kg^{-1}) was converted to ^{232}Th activity, which is independent of any Ra loss. Inter-method bias was checked by comparing the activity measured as ^{228}Ra with that measured as ^{232}Th, the latter being measured by ICP-MS on three reference materials from the IAEA-375 series (5 samples), IAEA-312 series (5 samples), and IAEA-RGTh-1 series (10 samples) and found to be 1.012 ± 0.026. Every ten samples, the IAEA-375 soil was counted, and results were within ±6 % (ζ-scores from −1.62 to 1.37) of the recommended value. The combined standard uncertainties were assessed using GUM, and decision threshold and detection limit were calculated based on ISO 11929-1 [44] (Table 4). Detection limits were 2.1, 0.6, 0.9, 0.5 and 6 Bq kg^{-1} for ^{238}U, ^{226}Ra, ^{228}Ra, ^{228}Th and ^{40}K, and the detection limit of the ICP-MS ^{232}Th determination was 0.17 Bq kg^{-1} (Table 4); all samples

exceeded them. The uncertainties of the activity ratio were propagated using Monte Carlo simulation (2×10^5 draws) assuming that the efficiency-calibration components common to both nuclides are fully correlated. External hazard indices were computed and compared with previous surveys [17, 18]:

$$Ra_{eq} = A_{Ra} + 1.43A_{Th} + 0.077A_K \quad (2)$$

$$D\ (nGy\ h^{-1}) = 0.462A_{Ra} + 0.604A_{Th} + 0.0417A_K \quad (3)$$

$$AEDE\ (mSv\ y^{-1}) = D \times 8760\ h \times 0.2 \times 0.7\ Sv\ Gy^{-1} \times 10^{-6} \quad (4)$$

where A_{Th} is the average of the activities of ^{228}Ac and ^{212}Pb/^{208}Tl.

Alpha spectrometry of uranium isotopes

The ratio of ^{234}U/^{238}U was determined in a stratified sub-set of 18 solids (6 per age class and 2 per district and class where available) and the associated pH 4, 168 h leachates. The same procedure was followed as for ICP-MS and only the 250 mL of pooled triplicate leachate remaining after the aliquot for ^{226}Ra was collected was evaporated for the leachates. Prior to digestion samples were spiked with ^{232}U (≈ 30 mBq, NIST-traceable). UTEVA resin (Eichrom) [45] was used for uranium separation, Th (including ^{228}Th grown in from the tracer) is eluted in 5 M HCl and U is stripped in 0.01 M HCl, co-precipitated on 0.1 μm filters and counted for 300,000 s on 450 mm^2 PIPS detectors (Mirion Alpha Analyst). Chemical recoveries were 71.6 ± 9.4 % (range 52.3–88.1 %) and peak resolution was 19–31 keV FWHM. The background of less than 0.2 mBq ^{238}U was obtained in procedural blanks. Each ^{234}U and ^{238}U peak contained at least 312 counts, and ^{238}U from alpha spectrometry agreed with ICP-MS within ±8.3 % (slope 0.974, r = 0.968, n = 18). Accuracy was verified with IAEA-385, for which ^{234}U/^{238}U was 0.987 ± 0.035 (n = 3) against a recommended value of 1.00.

Radon emanation

The emanation coefficient of the ^{222}Rn (ε) was measured for the same 18 sub-samples using the sealed/unsealed gamma method [46, 47]. Each sample was first conditioned to 10 ± 1 wt% moisture to standardise pore-water effects [48]; the ^{214}Pb/^{214}Bi activity was then measured immediately after packing (unsealed) and again after 30 days in the sealed container. The activity

ratio ε = 1 − Aunsealed/Asealed was calculated, where A is the mean $^{214}Pb/^{214}Bi$ activity. The uncertainties from counting statistics ranged from 0.011 to 0.027 absolute.

Batch leaching and selective extraction

Tropical rainfall (Na^+ 30, Ca^{2+} 12, Mg^{2+} 5, K^+ 4, Cl^- 40, SO_4^{2-} 18 and NO_3^- 14 μmol L^{-1}) was adjusted to pH 4.0, 6.0 or 8.0. Tailings (50 g) and solution (500 mL) (1:10) were mixed and rotated end-over-end at 30 rpm and at 25 ± 1 °C, with separate bottles being sacrificed at 24, 72 and 168 h, in triplicate. The pH at the start was not maintained and the tailings could buffer the solution as in the field, and pH at the end was measured. Leachates were centrifuged, filtered (0.45 μm) and acidified. The detection limits (d.l.) for U and Th were 0.005 and 0.002 μg L^{-1}, respectively, by ICP-MS. 400 mL of water was pre-concentrated onto MnO_2 [49] for the determination of ^{226}Ra by ^{222}Rn emanation and liquid scintillation counting (Quantulus GCT 6220, detection limit 4 mBq L^{-1}). Release percentages are based on the amount of material held in the solid phase. A five-step selective extraction method adapted from the Tessier [50] and BCR schemes, where an extra oxalate step was added, was performed for the 18 sub-samples: exchangeable (1 M NH_4OAc at pH 7, 2 h); acid-soluble (1 M NaOAc/HOAc at pH 5, 5 h); poorly crystalline Fe oxyhydroxides (0.2 M ammonium oxalate at pH 3, dark for 4 h); crystalline Fe oxides (dithionite–citrate–bicarbonate at 80 °C); and residual (F5, reported by difference from the total; the final residue was also fused and analysed to check recovery). U in extracts, measured by ICP-MS, was done using MnO_2 pre-concentration, and ^{226}Ra, measured by LSC, using pre-concentration by MnO_2. Recoveries (calculated as the ratio of the sum of F1–F4, plus a fused residue, to the total) of U and ^{226}Ra were 90.6–107.9 % and 86.8–111.4 %, respectively. Barite is not dissolved by these reagents and so the Ra found in F5 includes barite-hosted Ra as well as in silicates [24, 51].

Disequilibrium model

When ^{228}Ra is removed at a first-order rate k_{Ra}, and ^{232}Th is not mobile, ^{228}Ra will reach a steady state in a few multiples of $1/(\lambda_{228} + k_{Ra}) \approx 8$ y:

$$^{228}Ra/^{232}Th = \lambda_{228}/(\lambda_{228} + k_{Ra}),\ k_{Ra} = \lambda_{228}(^{232}Th/^{228}Ra - 1) \quad (5)$$

with $\lambda_{228} = 0.1205\ y^{-1}$.

For the intermediate deposits (5.5–18.5 y), $(\lambda_{228} + k_{Ra})t \approx 0.7–2.4$, i.e. only 50–91 % of the approach to steady state, so Eq. (5) gives a lower bound of k_{Ra}; for deposits older than 20 years,

$(\lambda_{228} + k_{Ra})t \geq 2.8$ ($\geq$ 94 % of steady state) and Eq. (5) applies. The decay of ^{226}Ra (t1/2 = 1600 y) does not reach a new steady state within the typical depositional age of decades and ingrowth of ^{226}Ra from ^{230}Th over this period is small enough to be neglected, so that $^{226}Ra/^{238}U$ represents the accumulation of the difference between the losses of Ra and U since deposition. If both nuclides were in equilibrium at deposition (proven to be the case for young tailings, below), and if kRa is the same for both isotopes of Ra, then the U loss rate constant is

$$k_U = k_{Ra} + \ln(^{226}Ra/^{238}U)/t \quad (6)$$

where t is the age of the deposit. Since there is approximately 7 % uncertainty on individual $^{228}Ra/^{232}Th$ ratios (Table 4), Eqs. (5) and (6) were applied to the class means rather than to individual deposits. To reduce the influence of extreme ratios, outliers were detected using Grubbs' test and results are presented both with and without outliers. In this context, the term 'loss' refers to the loss from the 0–30 cm layer sampled, which can be through downward redistribution and/or export from the facility.

Statistical analysis

The Shapiro–Wilk and Levene tests were used to assess the normality and homogeneity of variance. One-way ANOVA with Tukey's HSD test and/or Kruskal–Wallis test was used to verify age-class differences. Due to the fact that samples within the same district are not completely independent, and each sample was leached at three pH values, age effects tests were also conducted using linear mixed models (district, or sample, as random intercept). Log transformation of U release was used and subjected to a two-way ANOVA (age class x initial pH). Pearson and partial correlations, principal component analysis (PCA) on 24 standardised variables (sampling adequacy checked with the Kaiser–Meyer–Olkin statistic and Bartlett's test), non-linear least-squares regression and multiple linear regression were computed in Python 3.11 (SciPy 1.13, statsmodels 0.14, scikit-learn 1.5). Leave one site out (LOSO) cross-validation was performed to

validate the regression model, with each district left out one time, and R^2 and RMSE were calculated on the pooled out-of-fold predictions. The level of significance used was $\alpha = 0.05$.

Results and Discussion

Mineralogical evolution: three weathering stages

There was a significant difference between age classes in terms of paste pH ($F = 46.5$, $p < 0.001$; Table 1). Young tailings were near-neutral to alkaline (6.71 ± 0.72), intermediate tailings acidic and variable (4.79 ± 0.68, range 3.46–5.97) and aged tailings moderately acidic (5.41 ± 0.40). The buffered stage can reach its end point in a few years in some young deposits of Tarkwa–Prestea where carbonate content was low with the deposit already acidified to paste pH 4.17. Sulfide S fell from 0.97 to 0.10 wt% and SOI rose from 0.24 to 0.53. pool as a result of losses of carbonates and chlorite, and Feo increased by approximately 3.9-fold as Fe released by sulfide oxidation precipitated as poorly crystalline oxyhydroxides. TWI averaged 0.08, 0.26 and 0.52 and correlated with deposit age ($r = 0.76$, $p < 0.001$). Age effect on SOI, Feo, ^{238}U and $^{226}Ra/^{238}U$ were confirmed using the mixed models with district as the random intercept ($p \leq 0.001$).

Table 1 Physicochemical properties of tailings by age class (mean ± SD)

Parameter	Young (n = 20)	Intermediate (n = 20)	Aged (n = 14)	F (ANOVA)
Paste pH	6.71 ± 0.72	4.79 ± 0.68	5.41 ± 0.40	46.5***
EC, µS cm^{-1}	1396 ± 735	1422 ± 531	1182 ± 415	0.77 ns
Clay (<2 µm), %	5.8 ± 0.4	7.3 ± 1.0	9.5 ± 1.7	51.3***
S_{total}, wt%	1.25 ± 0.53	0.68 ± 0.26	0.18 ± 0.12	36.4***
$S_{sulfide}$, wt%	0.97 ± 0.52	0.46 ± 0.26	0.10 ± 0.11	25.9***
$S_{sulfate}$, wt%	0.28 ± 0.17	0.22 ± 0.10	0.08 ± 0.04	11.2***
SOI	0.24 ± 0.14	0.35 ± 0.17	0.53 ± 0.25	10.1***
Fe_2O_3, wt%	6.18 ± 1.11	6.86 ± 1.16	8.63 ± 2.01	12.7***
CaO, wt%	1.37 ± 0.81	0.62 ± 0.24	0.23 ± 0.08	22.1***
MgO, wt%	1.55 ± 0.31	1.23 ± 0.24	0.74 ± 0.31	32.6***
K_2O, wt%	2.11 ± 0.38	2.01 ± 0.35	1.41 ± 0.31	17.9***
As, mg kg^{-1}	786 ± 847	420 ± 465	105 ± 87	5.59**
Fe_o, g kg^{-1}	1.9 ± 0.8	4.0 ± 1.5	7.3 ± 1.8	62.0***
TWI	0.08 ± 0.11	0.26 ± 0.18	0.52 ± 0.26	23.6***

* $p < 0.05$; ** **$p < 0.01$;** *** $p < 0.001$; ns, not significant.

Young tailings had an average of 1.29 wt% carbonates, intermediate tailings had a median of 0.12 wt% (maximum 0.65 wt%) and 12 of the 14 aged samples had carbonates below detection (Table

2, Fig. 2). The pyrite content dropped from 1.73 to 0.15 wt%, and the amount of goethite rose to 3.55 ± 0.84 wt%, while the content of chlorite and feldspar decreased by about half. The Feo correlated with the X-ray amorphous fraction ($r = 0.91$, $p < 0.001$), while goethite correlated with Feo ($r = 0.86$, $p < 0.001$) consistent with the ripening of ferrihydrite to goethite. Jarosite was not detected; the lowest pH of the paste was 3.46 which is not within the stability field of jarosite, so schwertmannite and ferrihydrite are the expected Fe(III) precipitates [29, 52, 53]. The SEM-EDS revealed unaltered pyrite in young tailings, porous Fe oxyhydroxide rims (2–15 μm thick) in intermediate tailings, and Fe oxyhydroxide pseudomorphs with grain coatings in the aged tailings. In all classes, the primary hosts of Th, monazite and zircon were found intact.

Table 2 Mineral composition of tailings by age class (Rietveld, wt%, mean ± SD)

Phase	**Young**	**Intermediate**	**Aged**	**F**
Quartz	56.6 ± 3.1	55.9 ± 4.6	56.2 ± 3.8	0.16 ns
Muscovite/sericite	12.2 ± 2.3	10.8 ± 2.0	9.0 ± 1.6	10.2***
Chlorite	5.3 ± 1.6	4.4 ± 1.3	2.2 ± 1.1	22.6***
Kaolinite	2.7 ± 0.6	5.0 ± 1.5	8.9 ± 2.4	64.4***
Feldspars	6.0 ± 1.8	5.9 ± 1.4	3.3 ± 1.0	16.6***
Carbonates	1.29 ± 1.16	0.15 ± 0.18	0.02 ± 0.05	17.4***
Pyrite	1.73 ± 0.93	0.80 ± 0.47	0.15 ± 0.20	25.9***
Arsenopyrite	0.18 ± 0.21	0.08 ± 0.07	0.01 ± 0.01	6.96**
Hematite	2.7 ± 0.9	2.7 ± 1.0	2.9 ± 1.3	0.22 ns
Goethite	0.54 ± 0.41	1.60 ± 0.57	3.55 ± 0.84	103.1***
Gypsum	1.34 ± 0.88	1.00 ± 0.54	0.20 ± 0.13	13.8***
X-ray amorphous	6.6 ± 0.9	8.7 ± 2.4	11.0 ± 2.1	22.4***

Values below the detection limit set to zero for averaging; * $p < 0.05$; ** **$p < 0.01$;** *** $p < 0.001$; ns, not significant

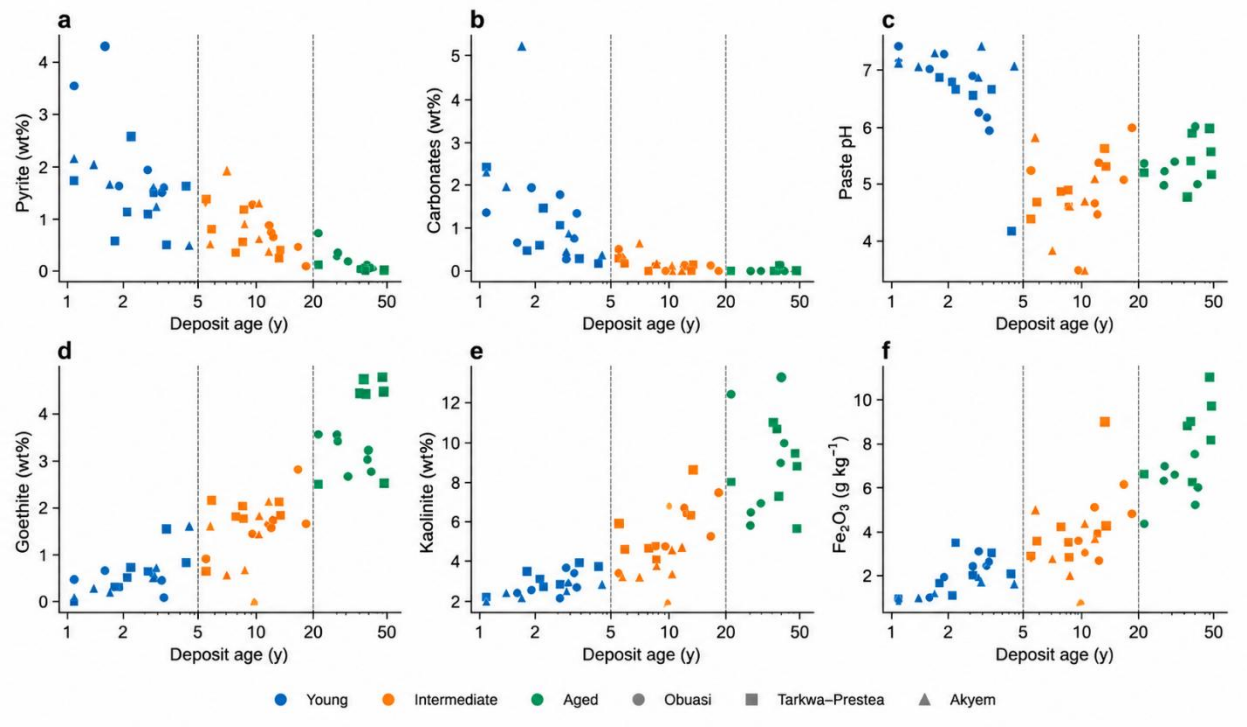


Fig. 2 Evolution of reactive minerals and paste pH with deposit age (log scale): a pyrite; b carbonates; c paste pH; d goethite; e kaolinite; f oxalate-extractable Fe. Dashed lines mark the class boundaries at 5 and 20 years.

These data indicate that there are three stages (summarised in Fig. 6). Process lime and primary carbonates are present in stage I, maintaining the pore water at near neutral pH, or more precisely around 7. Once the carbonate reserve in the deposits has been depleted (stage II occurs in most deposits within 5-10 years) the tailing water becomes acidic due to the oxidation of pyrite [54, 55]. During stage III the sulfide is almost completely depleted, pH approaches 5–6 and poorly crystalline Fe phases mature to goethite [52]. The surface 30 cm experienced approximately 92 % removal of pyrite in about 30 years, a rate of change that is very fast when compared to the typical rate of advance of oxidation fronts in temperate tailings [4, 30].

Activity concentrations and measurement uncertainty

The mean activity concentrations (Table 3) were in the range observed in soils around the world [17]. ^{238}U decreased with age from 28.3 ± 5.1 to 17.0 ± 4.5 Bq kg^{-1} ($F = 18.1$, $p < 0.001$); young and intermediate tailings did not differ (Tukey $p = 0.33$), whereas aged tailings differed from both. ^{226}Ra also decreased, but less (28.5 ± 4.3 to 22.1 ± 4.3 Bq kg^{-1}). ^{232}Th was found to be not related

to age ($p = 0.474$) but was associated with district with an average value of 44.6 Bq kg^{-1} at Tarkwa–Prestea, 27.0 at Obuasi and 29.0 at Akyem, the latter being a relatively less heavy-mineralized area. As a result of weathering of the feldspar and mica, ^{40}K decreased from 539 to 367 Bq kg^{-1}. Absorbed dose rates (36.7–74.0 nGy h^{-1}) and Ra_{eq} (77.2–161.0 Bq kg^{-1}) were not significantly higher than reference levels and all the radionuclides in the U and Th series were below the exemption level of 1 Bq g^{-1} [56].

Table 3 Activity concentrations (Bq kg^{-1}), disequilibrium ratios and radiological indices by age class (mean ± SD)

Quantity	Young	Intermediate	Aged	F (p)
^{238}U	28.3 ± 5.1	25.8 ± 6.5	17.0 ± 4.5	18.1 (<0.001)
^{226}Ra	28.5 ± 4.3	26.5 ± 5.7	22.1 ± 4.3	7.09 (0.002)
^{228}Ra (^{228}Ac)	33.7 ± 11.0	31.7 ± 9.0	34.3 ± 10.7	0.32 (0.725)
^{228}Th (^{212}Pb, ^{208}Tl)	33.2 ± 11.0	33.0 ± 8.9	35.4 ± 10.5	0.27 (0.768)
^{232}Th (ICP-MS)	33.1 ± 10.3	33.6 ± 9.1	37.1 ± 10.9	0.76 (0.474)
^{40}K	539 ± 107	516 ± 89	367 ± 82	15.2 (<0.001)
^{226}Ra/^{238}U	1.015 ± 0.097	1.041 ± 0.103	1.440 ± 0.676	7.14 (0.002)
^{228}Ra/^{232}Th	1.017 ± 0.056	0.943 ± 0.069	0.922 ± 0.066	11.1 (<0.001)
D, nGy h^{-1}	55.8 ± 7.0	53.3 ± 4.7	46.6 ± 4.7	11.4 (<0.001)
AEDE, mSv y^{-1}	0.068 ± 0.009	0.065 ± 0.006	0.057 ± 0.006	11.4 (<0.001)
Ra_{eq}	117.8 ± 16.0	112.5 ± 11.4	100.2 ± 11.6	7.33 (0.002)

World soil medians: ^{238}U 35, ^{232}Th 30, ^{40}K 400 Bq kg^{-1}; Ra_{eq} limit 370 Bq kg^{-1} [17, 18]

The uncertainty budget was assessed in detail for the chronometers (Table 4), as they are based on small departures from unity. The uncertainty for ^{238}U is dominated by counting statistics and the ^{234}Th self-absorption correction while the uncertainties for ^{226}Ra and ^{228}Ra are dominated by efficiency calibration and coincidence summing. The combined relative uncertainty of a single

339 $^{228}Ra/^{232}Th$ ratio (6.9 %) is similar to the decrease between young and aged tailings (9 %), and
340 hence, the ratio was interpreted as being at the level of the class means and not single deposits.

341 **Table 4** Relative standard uncertainty budget (%, k = 1) for a typical sample and ISO 11929
342 characteristic limits

Component	^{238}U ($^{234}Th/^{234m}Pa$)	^{226}Ra ($^{214}Pb/^{214}Bi$)	^{228}Ra (^{228}Ac)	^{232}Th (ICP-MS)
Counting statistics / repeatability	6.2	1.9	3.3	2.7
Efficiency calibration	2.8	2.4	2.4	2.2
Emission probability	2.6	0.6	0.9	–
Self-attenuation / density	3.9	1.3	0.7	–
Coincidence summing	–	1.6	2.1	–
Interferences / Rn leakage	1.7	0.9	–	–
Digestion recovery	–	–	–	3.6
Combined	8.4	3.8	4.7	5.0
Decision threshold, Bq kg^{-1}	1.04	0.29	0.43	0.08
Detection limit, Bq kg^{-1}	2.1	0.6	0.9	0.17

343 Characteristic limits per ISO 11929-1 [44] for 86,400 s counting and 350 g samples

344 ***Disequilibrium chronometry: rates of uranium and radium loss***

345 The secular equilibrium of young tailings ($^{226}Ra/^{238}U$ = 1.015 ± 0.097; one-sample t-test against
346 unity p = 0.490) demonstrates that there was no measurable fractionation of U from Ra due to
347 cyanidation, and validates the initial condition of Eq. (6). The ratio was hardly changed in
348 intermediate tailings (1.041 ± 0.103; 13 of 20 within 10 % of unity) but rose to 1.440 ± 0.676 in
349 aged tailings (Fig. 3a), correlating with ln(age) (r = 0.42, p = 0.002) and goethite (r = 0.53, p <
350 0.001). One extreme value (3.67) was found in the aged class (Grubbs' test (G) = 3.30; critical
351 value (G) = 2.51) and the aged mean is 1.269 without this value. The $^{228}Ra/^{232}Th$ ratio declined
352 from 1.017 ± 0.056 to 0.943 ± 0.069 and 0.922 ± 0.066 (Fig. 3b; F = 11.1, p < 0.001; r = −0.52, p
353 < 0.001 with ln(age)). Both older classes were significantly lower than young tailings (Tukey p =
354 0.0017 and 0.0002), but not significantly different from each other (p = 0.59), while the young
355 mean was not significantly different from unity (p = 0.185). Thorium itself is a stable internal
356 reference as the ^{232}Th was measured separately and the hosts were left unchanged during the

procedure.

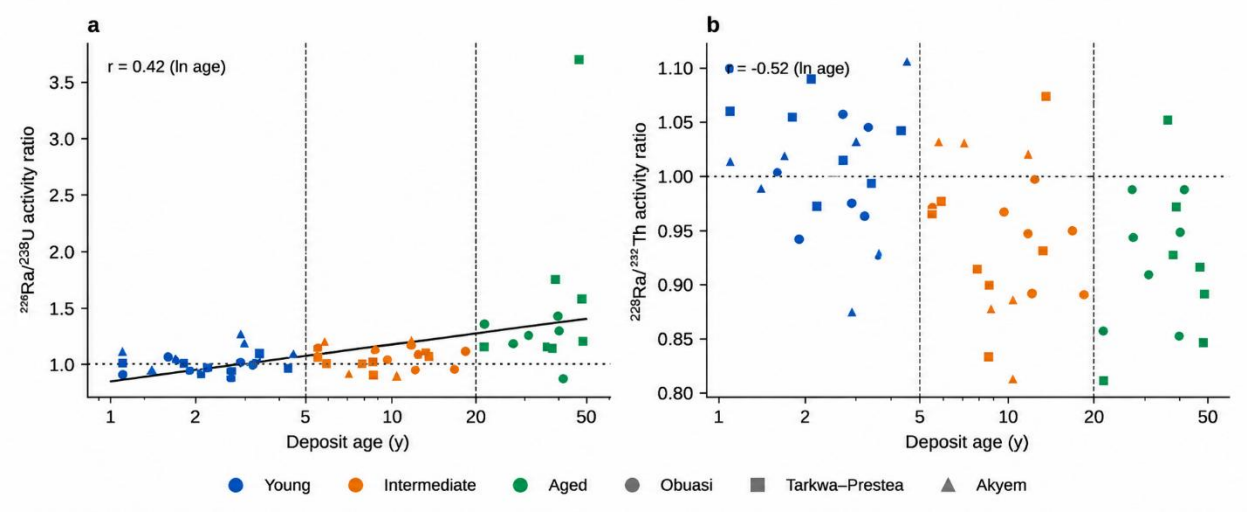


Fig. 3 Disequilibrium ratios against deposit age: a $^{226}Ra/^{238}U$ with the fit 0.845 + 0.141 ln(age); b $^{228}Ra/^{232}Th$. Colours denote age class and symbols district. Dotted lines mark secular equilibrium.

The value of kRa for aged tailings is close to steady state, and is estimated to be 1.0×10^{-2} y^{-1} (95 % CI 5.5×10^{-3} to 1.5×10^{-2}, propagated from the standard errors of the class means), or approximately 1 % per year of the radium inventory, while the intermediate-class value of 7.2×10^{-3} y^{-1} is a lower bound because steady state has not yet been reached. The $^{228}Th/^{228}Ra$ ranged from 0.99 to 1.05, slightly higher than unity in the older classes as would be expected if immobile ^{228}Th was being built from depleted ^{228}Ra, confirming that the ^{228}Ra deficit was not an artefact of the ^{228}Ac peak. Inserting the aged-class k_{Ra}, $^{226}Ra/^{238}U$ and mean age (36.2 y) into Eq. (6) gives $kU = 2.0 \times 10^{-2}$ y^{-1} (95 % CI 1.1×10^{-2} to 2.8×10^{-2}). Removing the outlier reduces this to 1.7×10^{-2} y^{-1} and normalising both ratios to the young-tailings means, which removes any constant bias between gamma spectrometry and ICP-MS, results in $kRa = 1.3 \times 10^{-2}$ and $kU = 2.2 \times 10^{-2}$ y^{-1}. Over 36 years these constants predict losses of 31–36 % of ^{226}Ra and 46–55 % of ^{238}U. The differences between young and aged tailings were found to be 22 % for ^{226}Ra and 40 % for ^{238}U (36 % at Obuasi and 49 % at Tarkwa–Prestea). The chronometers thus convey the direction as well as the degree of changes in the inventories, but they overestimate the losses, by a factor of about 1.4–1.6 for ^{226}Ra and 1.2–1.4 for ^{238}U. Three effects can be considered: averaging ratios that vary widely between deposits causes class means to be inflated (Jensen's inequality), ^{228}Ra produced by alpha recoil is probably more labile than ^{226}Ra, so that k_{Ra} for ^{226}Ra is overestimated, and the class-wide measured decline is biased low because Akyem tailings have a lower ^{238}U (24.5 Bq

379 kg^{-1}) than in the two districts that have aged tailings, in which the declines were larger. The
380 estimates are thus to be interpreted as upper limits of losses.

381 ***Leaching behaviour***

382 The final pH values were not congruent with the initial pH values (Table 5). Young tailings raised
383 the pH 4 solutions to an average final pH of 6.42, whereas intermediate tailings lowered the pH 8
384 solutions to 5.12 on average. In a two-way ANOVA on log-transformed U release (162 sample–
385 pH combinations), age class was significant ($F = 34.3$, $p < 0.001$) but initial pH was not ($F = 1.99$,
386 $p = 0.141$; interaction $p = 0.938$). A mixed model (with a random intercept for "sample") removed
387 between-sample variance and found a very small effect of initial pH ($p = 0.036$) in addition to the
388 strong age effect ($p < 0.001$); the buffering capacity of the tailings, rather than the acidity of the
389 rain, determined the pH of the leaching.

390 **Table 5** Final pH, radionuclide release after 168 h (% of solid inventory) and leachate $^{234}U/^{238}U$
391 (mean ± SD)

Class	Initial pH	Final pH	U	Th	^{226}Ra	$^{234}U/^{238}U$
Young	4	6.42 ± 0.76	1.88 ± 1.37	0.010 ± 0.006	1.37 ± 0.52	1.118 ± 0.071
	6	6.72 ± 0.75	1.65 ± 0.91	0.011 ± 0.005	1.37 ± 0.49	–
	8	6.99 ± 0.71	1.32 ± 0.42	0.008 ± 0.003	1.24 ± 0.51	–
Intermediate	4	4.41 ± 0.68	2.89 ± 2.32	0.018 ± 0.013	1.61 ± 0.42	1.047 ± 0.039
	6	4.78 ± 0.68	2.40 ± 1.14	0.016 ± 0.006	1.29 ± 0.45	–
	8	5.12 ± 0.70	2.21 ± 1.40	0.015 ± 0.006	1.43 ± 0.50	–
Aged	4	4.99 ± 0.43	0.91 ± 0.37	0.014 ± 0.004	1.96 ± 0.59	1.287 ± 0.104
	6	5.36 ± 0.38	1.06 ± 0.46	0.012 ± 0.003	1.62 ± 0.55	–
	8	5.84 ± 0.47	0.85 ± 0.56	0.011 ± 0.003	1.57 ± 0.49	–

392 $^{234}U/^{238}U$ determined by alpha spectrometry on the 18-sample sub-set at initial pH 4 only

393 The mean U release from intermediate, young and aged tailings at initial pH 4 were 2.89 %, 1.88
394 % and 0.91 % respectively. Only the intermediate–aged contrast was significant (Tukey $p =$
395 0.0035) and the young and intermediate tailings did not differ ($p = 0.14$), as a few young deposits
396 had already started to acidify. The final pH dropped below about 4.0 for the six leachates, which
397 showed release of 1.5–9.4 % (Fig. 4a). For all initial pH values, young tailings had a release of
398 1.32–1.88 % which is in line with a carbonate buffering and uranyl–carbonate complexation at the
399 high end of the pH range [57, 58]. All samples had a release of less than 0.1 % thorium (maximum
400 release 0.063 %). There was no correlation between the release of Ra and uranyl in leachate; at pH

4, the release of Ra increased slightly from 1.37 % in young to 1.96 % in aged tailing water, possibly due to a decrease in sulfate in leachate which showed a negative correlation with Ra ($r = -0.57$, $p < 0.001$); gypsum $r = -0.57$, $p < 0.001$). On average 46 % of the 168 h release occurred within 24 h and 76 % within 72 h. The maximum concentration of U in the leachates was 19.4 µg L^{-1}, which is below the WHO provisional guideline of 30 µg L^{-1} [59] and two intermediate samples were higher than half of the guideline.

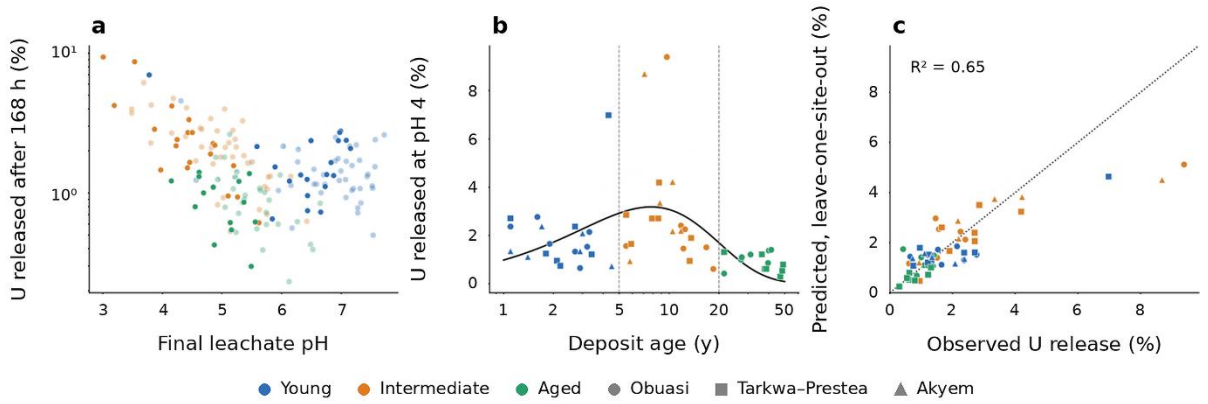


Fig. 4 Uranium mobility: a release after 168 h against final pH (lighter symbols for initial pH 6 and 8); b release at pH 4 against deposit age, with the fitted gamma-type curve; c leave-one-site-out validation of Eq. (7). Marker shapes denote districts.

Uranium isotopes, selective extraction and radon emanation: release mechanisms

Solid-phase $^{234}U/^{238}U$ decreased from 1.006 ± 0.027 in young to 0.981 ± 0.046 in intermediate and 0.932 ± 0.058 in aged tailings (Table 6), showing preferential loss of ^{234}U during weathering. The depletion is quantitatively consistent with the measured U loss: If 40 % of the U inventory has been lost with an integrated $^{234}U/^{238}U$ of ~1.10, a mass balance calculation predicts a remaining 0.934 against 0.932 measured. Leachate ratios indicate the release of U in each step. As is to be expected, a freshly milled surface (young tailings) showed a small excess of ^{234}U (1.118 ± 0.071). In intermediate tailings the ratio was near unity (1.047 ± 0.039), as expected if acid dissolves U hosts congruently. In aged tailings it increased to 1.287 ± 0.104 (range 1.153–1.468) reflecting that the small fraction still released is preferentially from α-recoil damaged sites and recoil-implanted ^{234}U at grain surfaces [25, 60] whilst the bulk of U remains locked within Fe phases. The aged-tailings leachate signature is similar to the range of $^{234}U/^{238}U$ obtained for groundwater and treated water around Obuasi [16] and could therefore be used as a tracer for the U that is

seeping from the oxidised tailings which are found in the local water system. This interpretation is confirmed by selective extraction (Table 6). The exchangeable fraction of U was the highest for intermediate tailings (9.3 % (most acidic at 21.7 %)) the acid soluble (carbonate associated) fraction decreased to a smaller fraction with age (20.6 % to 5.4 %); the poorly crystalline and crystalline Fe oxide associated fraction of U increased from 15.1 % in young tailings to 48.3 % in aged tailings. The Fe-oxide-associated Ra more than doubled with age (9.5 to 21.1 %), while the residual fraction (barite- and silicate-hosted Ra) was the most abundant (67.7–79.4 %). Radon emanation coefficients increased from 0.118 ± 0.031 to 0.163 ± 0.047 and 0.241 ± 0.058 and correlated with $^{226}Ra/^{238}U$ ($r = 0.68$, $p = 0.002$, $n = 18$). A higher emanation suggests that ^{226}Ra has been transferred from the mineral interiors to the grain surfaces where it is weakly sorbed onto Fe oxyhydroxides and clays [60, 62] and thus available for the slow continuous loss that is recorded by the $^{228}Ra/^{232}Th$ ratio.

Table 6 Uranium isotopes, operationally defined U and ^{226}Ra fractions and Rn emanation coefficients in the sub-set (n = 6 per class, mean ± SD)

Quantity	Young	Intermediate	Aged
$^{234}U/^{238}U$, solid	1.006 ± 0.027	0.981 ± 0.046	0.932 ± 0.058
$^{234}U/^{238}U$, leachate (pH 4)	1.118 ± 0.071	1.047 ± 0.039	1.287 ± 0.104
U F1 / F2 / F3 / F4 / F5, %	3.8 / 20.6 / 9.4 / 5.7 / 60.5	9.3 / 11.7 / 16.4 / 10.9 / 51.7	2.6 / 5.4 / 30.2 / 18.1 / 43.7
^{226}Ra F1 / F2 / F3 / F4 / F5, %	2.7 / 8.4 / 5.9 / 3.6 / 79.4	4.1 / 6.6 / 9.8 / 4.7 / 74.8	6.3 / 4.9 / 13.7 / 7.4 / 67.7
Rn emanation coefficient ε	0.118 ± 0.031	0.163 ± 0.047	0.241 ± 0.058

Fractions are means (SDs in Online Resource 1); F5 calculated by difference. F1 exchangeable; F2 acid-soluble; F3 oxalate-extractable Fe; F4 crystalline Fe oxides; F5 residual.

Controls on mobility and a predictive model

The PCA condenses the data set into a dominant weathering axis (Fig. 5). PC1 (45.6 % of the variance) contrasts the primary, buffered assemblage (carbonates, CaO, MgO, K_2O, chlorite, gypsum, sulfate, paste pH, ^{238}U and ^{226}Ra) with the products of oxidation (goethite, Fe_o, the X-ray amorphous fraction, Fe_2O_3, clay and SOI) and with $^{226}Ra/^{238}U$, so that sample scores move from young tailings on the left to aged tailings on the right. PC2 (11.5 %) is dominated by U and Ra release at pH 4; the highest PC2 scores belong to intermediate tailings, showing that U leachability

is not a monotonic function of weathering progress but peaks during the acid-reactive stage. ^{232}Th loads weakly on both components, consistent with its immobility. The close association of U with the Fe-oxide end-member is consistent with the strong sorption of U(VI) on ferrihydrite and goethite [63, 64]. Sampling adequacy was acceptable (KMO = 0.78; Bartlett's test $p < 0.001$).

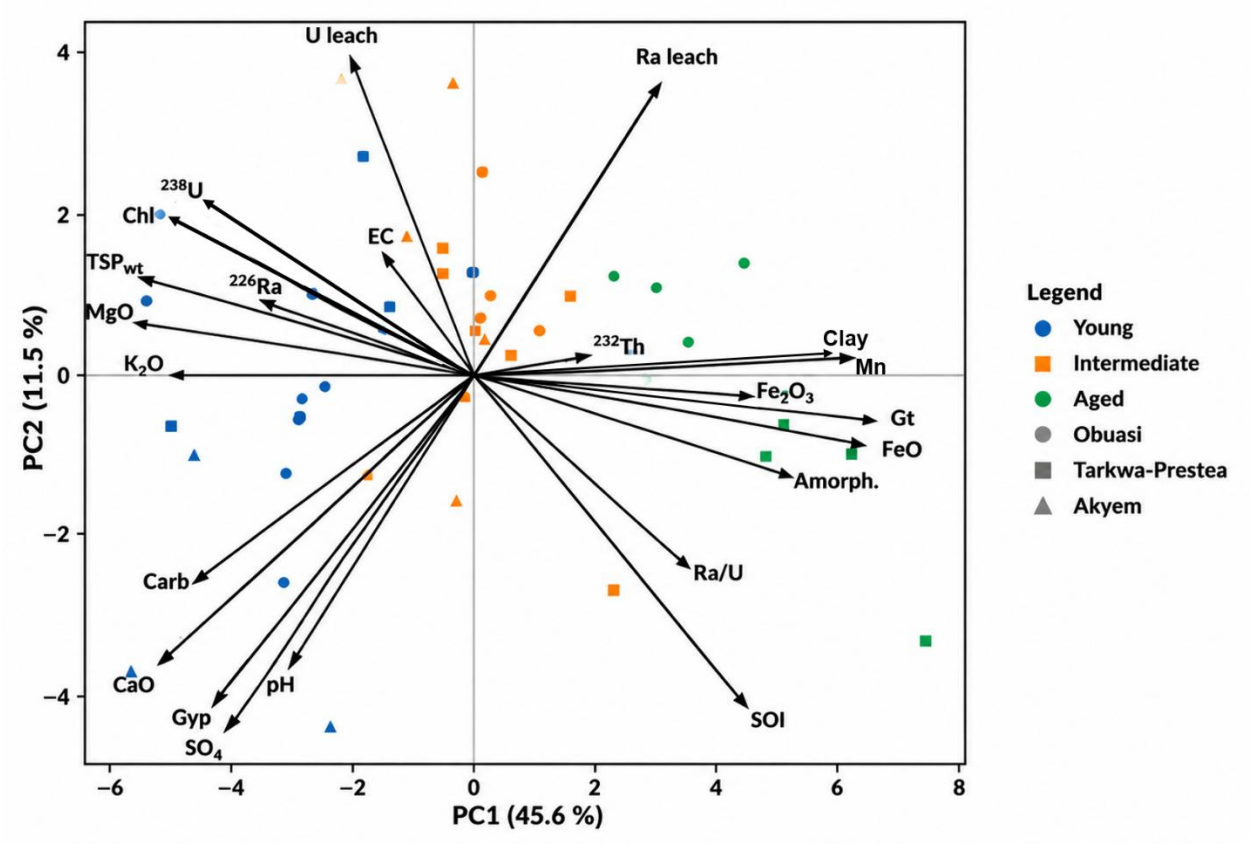


Fig. 5 PCA biplot of 24 variables for 54 tailings samples (PC1 oriented so that weathering increases to the right). SO_4 sulfate S; Carb carbonates; Chl chlorite; Gt goethite; Gyp gypsum; FeO oxalate-extractable Fe (Fe_o); Amorph. X-ray amorphous fraction; Ra/U ^{226}Ra/^{238}U; TSP_{wt} total S (wt%); Mn MnO (WD-XRF); leach, release at pH 4 and 168 h.

Release of uranium at pH 4 increased and then decreased with deposit age, a gamma-type function, $M(t) = A(t/\tau)\exp(1 - t/\tau)$ fit the data with $A = 3.2 \pm 0.3$ % and $\tau = 7.8 \pm 1.2$ y, but explained little

variance (R^2 = 0.22, Fig. 4b), as deposits of similar age weather at different rates. A model developed using data from routine laboratory analysis measurements worked much better:

$$\ln(\text{Urel}) = 3.87 - 0.457 \cdot \text{pHpaste} - 0.209 \cdot \text{Feo} \qquad (7)$$

with R^2 = 0.65 (both coefficients $p < 0.001$); adding SOI did not improve the fit ($p = 0.49$). Under LOSO cross-validation the pooled out-of-fold predictions gave R^2 = 0.65 (Fig. 4c); the out-of-fold RMSE was lowest when Tarkwa–Prestea was left out (0.74 %) and highest for Akyem (1.32 %). The most acidic samples were under-predicted by approximately half, so the model is reliable only for paste pH > ≈4 and underestimates U release from more acidic tailings.

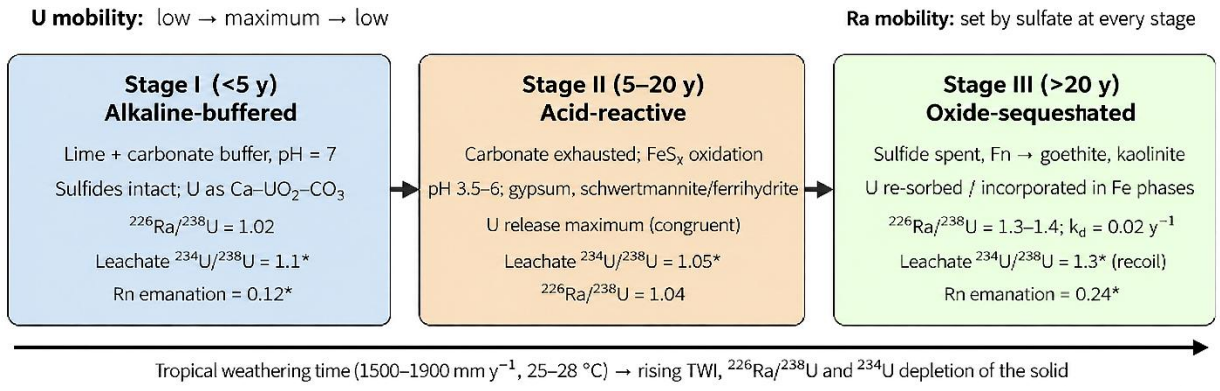


Fig. 6 Conceptual model of radionuclide behaviour in tropical gold tailings.

Comparison with other mining environments

The activity concentrations in the tailings from Ghana are comparable to those reported for other Ghanaian concessions [13, 15] and more than an order of magnitude lower than those of the uraniferous Witwatersrand tailings [8]. These materials by external dose criteria are not remarkable, but deposits with mean ^{238}U of only 26 Bq kg^{-1} yielded leachates containing up to 19 µg L^{-1} U due to the presence of labile U in significant amounts. Spatial variations of acid drainage caused by pyrite oxidation caused U and ^{226}Ra to be released at the Poços de Caldas uranium mine [65]; two decades after rehabilitation, acid U-bearing water was still being produced from the upper tailings at Mary Kathleen [31]; and in Nova Scotia, partially oxidised arsenopyrite is still present after 100 years of gold mining tailings [66]. The Ghanaian tailings reach comparable mineralogical endpoints within 20–30 years. The transfer of ^{228}Ra to the water

column from estuarine sediments draining artisanal gold-mining basins in Ghana [67] is consistent with the continuous loss of ^{228}Ra reported here.

Implications and limitations

The following are three points of practice. A first is that the time of maximum U mobility is the same time that many TSFs are closing, usually around 5-12 years after deposition (peak at 8 years), a time that cannot be predicted from surveys of fresh tailings. Maintenance of alkalinity after closure (by lime amendment or oxygen limiting cover in the first decade after closure) corrects the cause [68, 69] while reprocessing or artisanal mining of old tailings [70] may re-acidify causing a release of sorbed U. Second, the pH and Feo can be measured in any of the mine's laboratories, and Eq. (7) can be used to convert them to a convenient estimate of U leachability. Third, the $^{226}Ra/^{238}U$ and $^{228}Ra/^{232}Th$ ratios from routine gamma spectrometry are informative for loss rates and the leachate $^{234}U/^{238}U$ can relate tailings to water sources. Together they make NORM surveys informative not just for external dose. The results suggest that water quality and not exemption levels, should form the basis for regulating gold tailings, based on the WHO guideline on uranium levels in drinking water [59], within the framework of the Nuclear Regulatory Authority Act [71] The space-for-time design assumes that ore type and processing have not changed materially over the 50 years, so that the aged deposits started from a state similar to that of the present young tailings; this cannot be tested at Akyem, where no aged tailings exist. The first order losses and the same k_{Ra} for both isotopes of radium are assumed in equation (6). Since ^{228}Ra may be more labile than ^{226}Ra, k_{Ra} for ^{226}Ra, and consequently k_U, may be overestimated, which is consistent with the overprediction of measured losses reported above. Separation of the loss rates of the two isotopes ^{226}Ra and ^{228}Ra would be possible by depth resolved profiles. The 1:10 batch tests overestimate the water in contact with tailings and only the top 30 cm was sampled. The proposed mechanisms would be tested by depth profiling and by measuring $^{234}U/^{238}U$ in pore water and by synchrotron spectroscopy.

Conclusions

A 1–49 year chronosequence demonstrated that gold tailing samples from Ghana change from near-neutral, carbonate-buffered material to acidic, kaolinitic, goethite-rich residues within 2–3 decades, due to tropical weathering. The loss rate constants from the $^{226}Ra/^{238}U$ and the $^{228}Ra/^{232}Th$ chronometers are 1.7–2.2 × 10^{-2} y^{-1} for U and 1.0–1.3 × 10^{-2} y^{-1} for Ra, respectively, for aged

tailings, reproducing the direction and the magnitude of measured inventory losses, yet overestimating them, and best interpreted as upper bounds. Acid-reactive (intermediate) tailings had the highest release of uranium, significantly more than aged tailings, although not significantly more than young tailings, some of which had already begun to acidify; residual release was dominated by recoil-labile ^{234}U, and the leachate signature ($^{234}U/^{238}U = 1.29$) fell within the range reported for local groundwater (1.27–1.38). The release of radium was slightly greater for older ages, being correlated with the decrease of sulfate, while thorium remained preserved. The external radiological hazard of these tailings is close to world soil averages, whereas their water-borne hazard varies with weathering stage. As routine gamma spectrometry provides two radium chronometers the method can be applied to existing NORM survey data for sites where deposition ages are known, including surveys carried out in the past.

Acknowledgements We thank the managers of the participating mine fields for access to tailings facilities and records.

References

1. U.S. Geological Survey (2025) Mineral commodity summaries 2025. U.S. Geological Survey, Reston

2. Kossoff D, Dubbin WE, Alfredsson M, Edwards SJ, Macklin MG, Hudson-Edwards KA (2014) Mine tailings dams: characteristics, failure, environmental impacts, and remediation. Appl Geochem 51:229–245

3. Hudson-Edwards K (2016) Tackling mine wastes. Science 352:288–290

4. Blowes DW, Reardon EJ, Jambor JL, Cherry JA (1991) The formation and potential importance of cemented layers in inactive sulfide mine tailings. Geochim Cosmochim Acta 55:965–978

5. Nordstrom DK, Blowes DW, Ptacek CJ (2015) Hydrogeochemistry and microbiology of mine drainage: an update. Appl Geochem 57:3–16

6. Lindsay MBJ, Moncur MC, Bain JG, Jambor JL, Ptacek CJ, Blowes DW (2015) Geochemical and mineralogical aspects of sulfide mine tailings. Appl Geochem 57:157–177

7. IAEA (2003) Extent of environmental contamination by naturally occurring radioactive material (NORM) and technological options for mitigation. Technical Reports Series No. 419. IAEA, Vienna

8. Kamunda C, Mathuthu M, Madhuku M (2016) An assessment of radiological hazards from gold mine tailings in the province of Gauteng in South Africa. Int J Environ Res Public Health 13:138. https://doi.org/10.3390/ijerph13010138

9. Mathuthu M, Kamunda C, Madhuku M (2016) Modelling of radiological health risks from gold mine tailings in Wonderfonteinspruit catchment area, South Africa. Int J Environ Res Public Health 13:570. https://doi.org/10.3390/ijerph13060570

10. Mwimanzi JM, Haneklaus NH, Bituh T, Brink HG, Kiegiel K, Lolila F, Marwa JJ, Rwiza MJ, Mtei KM (2025) Radioactivity distribution in soil, rock and tailings at the Geita Gold Mine in Tanzania. J Radiat Res Appl Sci 18:101528. https://doi.org/10.1016/j.jrras.2025.101528

11. Nyarko BJB, Serfor-Armah Y, Holzbecher J, Osae EK, Akaho EHK, Carboo D, Chatt A (2003) Epithermal instrumental neutron activation analysis for the determination of gold and arsenic in Ghanaian gold tailings using conventional and anti-coincidence counting. J Radioanal Nucl Chem 256:253–257

12. Darko EO, Faanu A, Awudu AR, Emi-Reynolds G, Yeboah J, Oppon OC, Akaho EHK (2010) Public exposure to hazards associated with natural radioactivity in open-pit mining in Ghana. Radiat Prot Dosim 138:45–51

13. Faanu A, Ephraim JH, Darko EO (2011) Assessment of public exposure to naturally occurring radioactive materials from mining and mineral processing activities of Tarkwa Goldmine in Ghana. Environ Monit Assess 180:15–29

14. Gbadago JK, Faanhof A, Darko EO, Schandorf C (2011) Investigation of the environmental impacts of naturally occurring radionuclides in the processing of sulfide ores for gold using gamma spectrometry. J Radiol Prot 31:337–352. https://doi.org/10.1088/0952-4746/31/3/003

15. Faanu A, Adukpo OK, Tettey-Larbi L, et al (2016) Natural radioactivity levels in soils, rocks and water at a mining concession of Perseus gold mine and surrounding towns in Central Region of Ghana. SpringerPlus 5:98. https://doi.org/10.1186/s40064-016-1716-5

16. Awudu AR, Darko EO (2011) 234U/238U and 235U/238U ratios in domestic water from the environs of Obuasi mine in Ghana. J Radioanal Nucl Chem 287:129–134. https://doi.org/10.1007/s10967-010-0662-x

17. UNSCEAR (2000) Sources and effects of ionizing radiation. UNSCEAR 2000 Report to the General Assembly, with scientific annexes, vol I. United Nations, New York

18. Beretka J, Mathew PJ (1985) Natural radioactivity of Australian building materials, industrial wastes and by-products. Health Phys 48:87–95

19. Landa ER (2004) Uranium mill tailings: nuclear waste and natural laboratory for geochemical and radioecological investigations. J Environ Radioact 77:1–27

20. Abdelouas A (2006) Uranium mill tailings: geochemistry, mineralogy, and environmental impact. Elements 2:335–341

21. Chautard C, Beaucaire C, Gérard M, Roy R, Savoye S, Descostes M (2020) Geochemical characterization of uranium mill tailings (Bois Noirs Limouzat, France) highlighting the U and 226Ra retention. J Environ Radioact 218:106251

22. Lahrouch F, Guo N, Hunault MOJY, Solari PL, Descostes M, Gérard M (2021) Uranium retention on iron oxyhydroxides in post-mining environmental conditions. Chemosphere 264:128473. https://doi.org/10.1016/j.chemosphere.2020.128473

23. Landa ER (2003) Mobilization of radionuclides from uranium mill tailings and related waste materials in anaerobic environments. J Radioanal Nucl Chem 255:559–563. https://doi.org/10.1023/A:1022501003604

24. Besançon C, Chautard C, Beaucaire C, Savoye S, Sardini P, Gérard M, Descostes M (2020) The role of barite in the post-mining stabilization of radium-226: a modeling contribution for sequential extractions. Minerals 10:497

25. Chabaux F, Riotte J, Dequincey O (2003) U-Th-Ra fractionation during weathering and river transport. Rev Mineral Geochem 52:533–576

26. Dosseto A, Turner SP, Chappell J (2008) The evolution of weathering profiles through time: new insights from uranium-series isotopes. Earth Planet Sci Lett 274:359–371

27. Rihs S, Gontier A, Pelt E, Fries D, Turpault M-P, Chabaux F (2016) Behavior of U, Th and Ra isotopes in soils during a land cover change. Chem Geol 441:106–123. https://doi.org/10.1016/j.chemgeo.2016.08.016

28. Owusu K, Waylen P (2009) Trends in spatio-temporal variability in annual rainfall in Ghana (1951–2000). Weather 64:115–120

29. Dold B, Fontboté L (2001) Element cycling and secondary mineralogy in porphyry copper tailings as a function of climate, primary mineralogy, and mineral processing. J Geochem Explor 74:3–55

30. Moncur MC, Ptacek CJ, Blowes DW, Jambor JL (2005) Release, transport and attenuation of metals from an old tailings impoundment. Appl Geochem 20:639–659

31. Lottermoser BG, Ashley PM (2005) Tailings dam seepage at the rehabilitated Mary Kathleen uranium mine, Australia. J Geochem Explor 85:119–137. https://doi.org/10.1016/j.gexplo.2005.01.001

32. Smedley PL (1996) Arsenic in rural groundwater in Ghana. J Afr Earth Sci 22:459–470

33. Amonoo-Neizer EH, Nyamah D, Bakiamoh SB (1996) Mercury and arsenic pollution in soil and biological samples around the mining town of Obuasi, Ghana. Water Air Soil Pollut 91:363–373

34. Asante KA, Agusa T, Subramanian A, Ansa-Asare OD, Biney CA, Tanabe S (2007) Contamination status of arsenic and other trace elements in drinking water and residents from Tarkwa, a historic mining township in Ghana. Chemosphere 66:1513–1522

35. Bempah CK, Ewusi A (2016) Heavy metals contamination and human health risk assessment around Obuasi gold mine in Ghana. Environ Monit Assess 188:261

36. Allibone AH, McCuaig TC, Harris D, et al (2002) Structural controls on gold mineralization at the Ashanti belt, Obuasi, Ghana. In: Goldfarb RJ, Nielsen RL (eds) Integrated methods for discovery: global exploration in the twenty-first century. Soc Econ Geol Spec Publ 9:65–93

37. Pigois JP, Groves DI, Fletcher IR, McNaughton NJ, Snee LW (2003) Age constraints on Tarkwaian palaeoplacer and lode-gold formation in the Tarkwa-Damang district, SW Ghana. Miner Deposita 38:695–714. https://doi.org/10.1007/s00126-003-0360-5

38. Allibone A, Teasdale J, Cameron G, et al (2002) Timing and structural controls on gold mineralization at the Bogoso gold mine, Ghana, West Africa. Econ Geol 97:949–969. https://doi.org/10.2113/gsecongeo.97.5.949

39. Sobek AA, Schuller WA, Freeman JR, Smith RM (1978) Field and laboratory methods applicable to overburdens and minesoils. EPA-600/2-78-054. U.S. Environmental Protection Agency, Cincinnati

40. Canfield DE, Raiswell R, Westrich JT, Reaves CM, Berner RA (1986) The use of chromium reduction in the analysis of reduced inorganic sulfur in sediments and shales. Chem Geol 54:149–155

628 41. Schwertmann U (1964) Differenzierung der Eisenoxide des Bodens durch Extraktion mit
629 Ammoniumoxalat-Lösung. Z Pflanzenernähr Düng Bodenkd 105:194–202
630 42. Vidmar T (2005) EFFTRAN—a Monte Carlo efficiency transfer code for gamma-ray
631 spectrometry. Nucl Instrum Methods Phys Res A 550:603–608
632 43. Cutshall NH, Larsen IL, Olsen CR (1983) Direct analysis of 210Pb in sediment samples: self-
633 absorption corrections. Nucl Instrum Methods Phys Res 206:309–312
634 44. ISO (2025) ISO 11929-1:2025 Determination of the characteristic limits (decision threshold,
635 detection limit and limits of the coverage interval) for measurements of ionizing radiation —
636 Fundamentals and application — Part 1: Elementary applications. International Organization
637 for Standardization, Geneva
638 45. Horwitz EP, Chiarizia R, Dietz ML, Diamond H, Nelson DM (1992) Separation and
639 preconcentration of uranium from acidic media by extraction chromatography. Anal Chim
640 Acta 266:25–37. https://doi.org/10.1016/0003-2670(92)85276-C
641 46. IAEA (2013) Measurement and calculation of radon releases from NORM residues. Technical
642 Reports Series No. 474. IAEA, Vienna
643 47. Jha SK, Prusty P, Sahu A, et al (2021) Study on radon (222Rn) emanation coefficient and mass
644 exhalation rate from heavy minerals of high specific gravity. J Radioanal Nucl Chem 328:339–
645 346. https://doi.org/10.1007/s10967-021-07648-5
646 48. Huang C, Li S, Ye Y, Ding D, Wu W (2019) Variation rules of the radon emanation coefficient
647 in dump-leached uranium tailing sand. J Radioanal Nucl Chem 319:1037–1043.
648 https://doi.org/10.1007/s10967-018-06408-2
649 49. Eikenberg J, Tricca A, Vezzu G, Bajo S, Ruethi M, Surbeck H (2001) Determination of 228Ra,
650 226Ra and 224Ra in natural water via adsorption on MnO2-coated discs. J Environ Radioact
651 54:109–131
652 50. Tessier A, Campbell PGC, Bisson M (1979) Sequential extraction procedure for the speciation
653 of particulate trace metals. Anal Chem 51:844–851
654 51. Yousfi I, Bolle O, Geiss O (1999) Chemical extractions applied to the determination of radium
655 speciation in uranium mill tailing: study of different reagents. J Radioanal Nucl Chem
656 240:835–840

52. Bigham JM, Schwertmann U, Traina SJ, Winland RL, Wolf M (1996) Schwertmannite and the chemical modeling of iron in acid sulfate waters. Geochim Cosmochim Acta 60:2111–2121

53. Jamieson HE, Walker SR, Parsons MB (2015) Mineralogical characterization of mine waste. Appl Geochem 57:85–105

54. Singer PC, Stumm W (1970) Acidic mine drainage: the rate-determining step. Science 167:1121–1123

55. Williamson MA, Rimstidt JD (1994) The kinetics and electrochemical rate-determining step of aqueous pyrite oxidation. Geochim Cosmochim Acta 58:5443–5454

56. IAEA (2014) Radiation protection and safety of radiation sources: international basic safety standards. IAEA Safety Standards Series No. GSR Part 3. IAEA, Vienna

57. Bernhard G, Geipel G, Reich T, Brendler V, Amayri S, Nitsche H (2001) Uranyl(VI) carbonate complex formation: validation of the Ca2UO2(CO3)3(aq.) species. Radiochim Acta 89:511–518

58. Dong W, Brooks SC (2006) Determination of the formation constants of ternary complexes of uranyl and carbonate with alkaline earth metals (Mg2+, Ca2+, Sr2+, and Ba2+) using anion exchange method. Environ Sci Technol 40:4689–4695

59. WHO (2022) Guidelines for drinking-water quality: fourth edition incorporating the first and second addenda. World Health Organization, Geneva

60. Fleischer RL (1980) Isotopic disequilibrium of uranium: alpha-recoil damage and preferential solution effects. Science 207:979–981

61. Sajih M, Bryan ND, Livens FR, et al (2014) Adsorption of radium and barium on goethite and ferrihydrite: a kinetic and surface complexation modelling study. Geochim Cosmochim Acta 146:150–163. https://doi.org/10.1016/j.gca.2014.10.008

62. Méndez JC, Hiemstra T (2020) High and low affinity sites of ferrihydrite for metal ion adsorption: data and modeling of the alkaline-earth ions Be, Mg, Ca, Sr, Ba, and Ra. Geochim Cosmochim Acta 286:289–305

63. Waite TD, Davis JA, Payne TE, Waychunas GA, Xu N (1994) Uranium(VI) adsorption to ferrihydrite: application of a surface complexation model. Geochim Cosmochim Acta 58:5465–5478

686 64. Payne TE, Davis JA, Waite TD (1994) Uranium retention by weathered schists – the role of
687 iron minerals. Radiochim Acta 66/67:297–303
688 65. Fernandes HM, Franklin MR (2001) Assessment of acid rock drainage pollutants release in the
689 uranium mining site of Poços de Caldas – Brazil. J Environ Radioact 54:5–25
690 66. Walker SR, Parsons MB, Jamieson HE, Lanzirotti A (2009) Arsenic mineralogy of near-
691 surface tailings and soils: influences on arsenic mobility and bioaccessibility in the Nova
692 Scotia gold mining districts. Can Mineral 47:533–556
693 67. Klubi E, Abril JM, Mantero J, García-Tenorio R, Nyarko E (2020) Environmental radioactivity
694 and trace metals in surficial sediments from estuarine systems in Ghana (Equatorial Africa),
695 impacted by artisanal gold-mining. J Environ Radioact 218:106260.
696 https://doi.org/10.1016/j.jenvrad.2020.106260
697 68. Parbhakar-Fox A, Lottermoser BG (2015) A critical review of acid rock drainage prediction
698 methods and practices. Miner Eng 82:107–124
699 69. Dold B (2017) Acid rock drainage prediction: a critical review. J Geochem Explor 172:120–
700 132
701 70. Hilson G (2002) The environmental impact of small-scale gold mining in Ghana: identifying
702 problems and possible solutions. Geogr J 168:57–72
703 71. Republic of Ghana (2015) Nuclear Regulatory Authority Act, 2015 (Act 895). Ghana
704 Publishing Company, Accra